AJR American Journal of Roentgenology

Use of Photon-Counting Detector CT to Visualize Liver-Specific Gadolinium-Based Contrast Agents: A Phantom Study

Stephan Rau, MD[1], Thomas Stein, MSc[1], Alexander Rau, MD[2], Sebastian Faby, PhD[3], Maximilian F. Russe, MD[1], Gregor Jost, PhD[4], Michael C. Doppler, MD[1], Friederike Lang, BSc[1], Fabian Bamberg, MD, MPH[1], Hubertus Pietsch, PhD[4], Jakob Weiss, MD[1]

Gastrointestinal Imaging · Original Research

Available for this article:
CME credit
Editorial Comment by Zhou
Editorial Comment by Murakami

Keywords: contrast media, gadolinium, photon-counting CT, photon-counting detectors, x-ray computed

Submitted: Nov 23, 2024
Revision requested: Dec 13, 2024
Revision received: Jan 6, 2025
Accepted: Jan 23, 2025
First published online: Feb 5, 2025
Version of record: Apr 9, 2025

Siemens Healthineers provided technical support without control over the data. Bayer Pharma contributed the measurement of the dilution series in the mass spectroscope.

The authors declare that there are no disclosures relevant to the subject matter of this article.

BACKGROUND. The low clinically approved doses of gadolinium-based contrast agents (GBCAs) do not generate sufficient enhancement on CT for diagnostic purposes. Photon-counting detector (PCD) CT offers improved spectral resolution and could potentially enable visualization of hepatocyte-specific GBCAs, given their associated high gadolinium concentrations within hepatocytes.

OBJECTIVE. The purpose of this study was to investigate the potential of gadoxetate disodium in combination with PCD CT and low-energy virtual monoenergetic imaging (VMI) reconstructions to achieve an increase in attenuation in a phantom.

METHODS. A series of solutions was prepared of diluted gadoxetate disodium (concentrations of 0.250–2.5 μmol/mL, corresponding with doses of 25–200 μmol/kg). These solutions, along with deionized water, were evaluated in an anthropomorphic abdominal phantom using a clinical PCD CT scanner; VMI reconstructions at 40, 50, 60, and 70 keV and virtual noncontrast (VNC) imaging reconstructions were generated. Attenuation measurements were obtained; a linear regression model combined these values with previously reported in vivo data to estimate hepatic enhancement and CNR across doses.

RESULTS. Attenuation increased with increasing concentration at a given energy level and with decreasing energy level for a given concentration; VNC images had the lowest attenuation. The maximum attenuation reached in the abdominal phantom was 45.2 HU for a concentration of 2.5 μmol/mL at 40 keV. A concentration of 0.25 μmol/mL had attenuation at 40 keV of 13.0 HU. The model yielded estimated in vivo hepatic enhancement at 40 keV of 4.9 HU for a dose of 25 μmol/kg, 19.9 HU for 100 μmol/kg, and 30.8 HU for 200 μmol/kg; corresponding CNRs were 0.13, 0.52, and 0.81, respectively.

CONCLUSION. The combination of gadoxetate disodium and PCD CT could theoretically allow appreciable hepatic enhancement at a 200-μmol/kg dose; such effect was not observed for the clinically approved 25-μmol/kg dose.

CLINICAL IMPACT. PCD CT achieved attenuation increases for gadoxetate disodium at considerably lower doses than previously documented for CT of GBCAs, albeit at approximately eight times greater than clinical doses, which were thus too high for clinical use. Additional research exploiting PCD CT technology could seek to reduce further doses required for sufficient visualization into a clinically feasible range, to potentially allow CT using a liver-specific agent.

Currently, all clinically approved CT contrast agents are iodine-based, exploiting iodine's relatively high atomic number of 53 to achieve increased x-ray attenuation [1, 2]. These agents have short peak enhancement in tissue, typically up to 2 minutes after injection, potentially limiting their ability to characterize certain pathologic conditions through a single administration. Whereas administration of iodine-based contrast agents is safe in most patients, side effects including allergic reactions, hyperthyroidism, and nephropathy limit the total administered dose and/or the ability to administer repeated doses in a single examination [3, 4].

[1]Department of Diagnostic and Interventional Radiology, Medical Center, Faculty of Medicine, University of Freiburg, Hugstetter Str 55, 79106 Freiburg im Breisgau, Germany. **Address correspondence to** S. Rau (stephan.rau@uniklinik-freiburg.de).

[2]Department of Neuroradiology, Medical Center, Faculty of Medicine, University of Freiburg, Freiburg, Germany.

[3]CT, Siemens Healthineers, Forchheim, Germany.

[4]MR and CT Contrast Media Research, Bayer Pharma, Berlin, Germany.

doi.org/10.2214/AJR.24.32434
AJR 2025; 224:e2432434
ISSN-L 0361-803X/25/2244–e2432434
© American Roentgen Ray Society

Downloaded from www.ajronline.org by 186.248.128.23 on 05/21/25 from IP address 186.248.128.23. Copyright ARRS. For personal use only; all rights reserved

Downloaded from www.ajronline.org by 186.248.128.23 on 05/21/25 from IP address 186.248.128.23. Copyright ARRS. For personal use only; all rights reserved

Several studies have explored potential use of gadolinium-based contrast agents (GBCAs), which are typically used in MRI, as alternate contrast agents for CT [5–10]. Similar to iodine, gadolinium has a high atomic number of 64 and induces a concentration-dependent x-ray attenuation related to its mass density [11]. However, recommended clinical doses are approximately one hundredfold lower for GBCAs for MRI (e.g., 25–100 μmol/kg body weight, corresponding to 3.93–15.7 mg gadolinium per kg body weight) than for iodine-containing compounds for CT (e.g., 500–700 mg I per kg body weight) [12–16]. Given resulting low tissue concentrations of gadolinium, standard doses of GBCAs do not generate sufficient enhancement on CT for diagnostic purposes [5–7]. Indeed, in one study, doses of a GBCA of approximately 500 μmol/kg body weight were required to achieve increased hepatic attenuation on CT [10].

The recent clinical implementation of the first generation of photon-counting detector (PCD) CT systems has been accompanied by renewed interest in performing gadolinium-enhanced CT, with varying proposed applications including imaging using simultaneous administration of different contrast agents (i.e., gadolinium-based and iodine-based agents) [8, 12, 13, 17]. PCD CT systems use energy-resolving detectors that directly count the number of photons at different energy levels, facilitating energy discrimination and providing superior spectral resolution compared with earlier CT technologies. This greater spectral resolution in turn allows improved material differentiation and attenuation characterization at low energy levels, such as at 40 keV, at which GBCAs exhibit increases in attenuation [11, 14]. Despite such advantages, the ability to achieve meaningful CT image contrast using GBCAs has remained limited for PCD CT, due primarily to the low GBCA doses currently approved for clinical use.

The combination of a GBCA with PCD CT using low-energy reconstructions could have a potential novel application, distinct from previously explored applications, in liver imaging using hepatocyte-specific contrast agents [8, 15]. For some such compounds (e.g., gadoxetate disodium), approximately 50% of the administered dose is eliminated via the biliary system, resulting in a particularly high gadolinium concentration within hepatocytes and a plateaulike contrast enhancement between 20 and 300 minutes after administration [16, 18]. If they yield appreciable enhancement on CT, then hepatocyte-specific GBCAs could provide comparable advantages as are well-recognized for MRI, helping to overcome limitations of CT evaluation using current iodine-containing agents, all of which lack such specificity and wash out after a few minutes [19]. For example, long-lasting hepatic parenchymal enhancement could aid liver lesion characterization (e.g., identification of hepatocyte-free lesions [20]), and delayed visualization of the biliary system could aid characterization of biliary variants and injuries.

The manufacturer-recommended dose of gadoxetate disodium for routine clinical MRI examinations is 25 μmol/kg body weight, lower than for other GBCAs [13, 16, 21]. Nonetheless, the combination of this agent's high accumulation in hepatocytes and a PCD CT examination using dedicated postprocessing techniques (e.g., reconstruction of virtual monoenergetic imaging [VMI] at low energy levels) conceivably may provide sufficient hepatic parenchymal enhancement for diagnostic liver evaluation. Larger doses of gadoxetate disodium than the clinically approved dose (e.g., doses of 50–500 μmol/kg body weight) may also be tolerable, although there is a paucity of relevant data [10, 19–22].

The purpose of this study was to investigate the potential of gadoxetate disodium in combination with PCD CT and low-energy VMI reconstructions to achieve an increase in attenuation in a phantom.

Highlights

Key Finding

- *In this phantom study, PCD CT with gadoxetate disodium yielded progressive increases in attenuation at increasing concentrations. Estimated in vivo hepatic enhancement at 40 keV was 4.9 HU for the agent's clinically approved dose of 25 μmol/kg, versus 19.9 HU for 100 μmol/kg and 30.8 HU for 200 μmol/kg.*

Importance

- *PCD CT yielded meaningful attenuation increases for gadoxetate disodium at lower doses than previously documented for CT of GBCA, albeit too high for clinical use.*

Methods

One author (S.F.) is an employee of Siemens Healthineers. This author provided general technical support in the use of the PCD CT system, but had no role in the generation of study data. Two authors (G.J. and H.P.) are employees of Bayer Pharma. These authors conducted the measurement of the dilution series in the mass spectroscope (as described later in the Methods). The remaining authors, who are not employees of the previously noted companies, otherwise independently conducted the study design, data analysis, and data interpretation and had full control of the information submitted for publication.

Gadoxetate Disodium Dilution Series

A series of solutions was prepared, consisting of the hepatocyte-specific agent gadoxetate disodium (Primovist, Bayer Schering) diluted in deionized water to achieve varying gadoxetate disodium concentrations (measured in micromoles per milliliter of water). The concentration ranged from 0.00 to 2.5 μmol/mL. The gadolinium concentrations ranged 0.250 to 2.5 μmol/mL; this range was estimated to correspond with gadoxetate disodium doses ranging from 25 μmol/kg body weight (the routine clinical dose of gadoxetate disodium) to 200 μmol/kg body weight (a potentially tolerable larger dose). An additional solution was prepared with a gadolinium concentration of 0.00 μmol/mL (i.e., deionized water only). All solutions were prepared in a sterile environment using single-channel mechanical micropipettes having a volume range of 100–1000 μL (Eppendorf Research plus, Eppendorf).

To validate the preparation of the dilution series, the gadolinium content of each solution was measured using inductively coupled plasma-optical emission spectroscopy (ICP-OES) with a mass spectrometer (iCAP 7600 ICP-OES Duo, Thermo Fisher Scientific). Three aliquots were prepared from each gadoxetate disodium dilution by adding 50 μL of a 1000-ppm certified inductively coupled plasma calibration solution (Y, Merck) and a varying volume of 5% nitric acid (HNO_3) (125–500 μL, depending

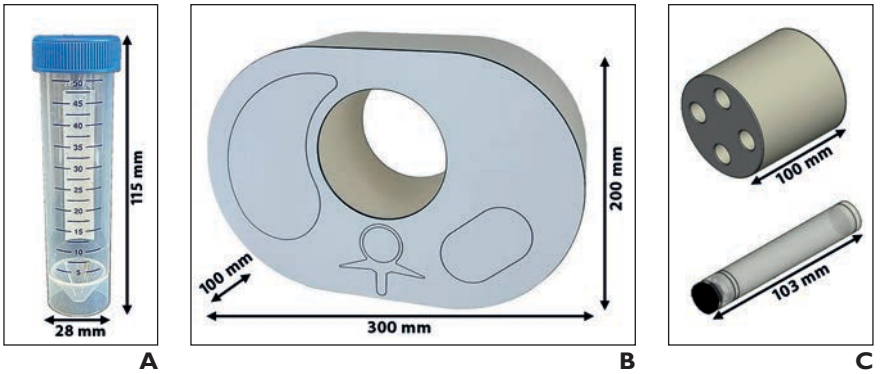

Fig. 1—Phantoms used in this study.
A, Photograph of custom-built phantom consisting of plastic stack containing 20 cylindric plastic centrifuge tubes with screw cap, capacity of 50 mL, length of 115 mm, and diameter of 28 mm.
B, Illustration shows anthropomorphic abdomen phantom (QRM-20118, QRM) measuring 200 × 300 mm × 100 mm. (Illustration © QRM; used with permission)
C, Illustration shows cylindric core (QRM-10139 spectral CT-phantom, QRM) designed for evaluation of spectral CT protocols. Core (*top*) measures 100 mm in diameter and contains refillable cylindric inserts (*bottom*) with diameter of 20 mm and length of 103 mm. (Illustration © QRM; used with permission)

on the gadoxetate disodium concentration), to generate a solution with a volume of 5 mL. Elemental quantification of gadolinium content was obtained from each aliquot using a 2-point calibration and Y as an internal standard; the mean value was obtained across the three aliquots for each dilution. The gadoxetate disodium concentrations of the original dilutions were then determined on the basis of the dilution factors.

Phantom Setup

The gadoxetate disodium dilution series was evaluated using two different phantoms, to assess differences in attenuation at varying concentrations. First, an in-house–developed custom phantom was used to evaluate the dilution series in a simplified setting with high image quality. Then, a commercial anthropomorphic abdominal phantom was used to simulate a clinical environment. The phantoms are displayed in Figure 1.

The custom phantom consisted of a plastic stack containing 20 cylindric plastic centrifuge tubes. Each tube had a screw cap, as well as a capacity of 50 mL, length of 11.5 cm, and diameter of 2.8 cm. The tubes were filled with 20 distinct dilutions having increasing concentrations of gadoxetate disodium ranging from 0.00 to 2.5 μmol/mL in increments of 0.125 μmol/mL. The anthropomorphic phantom (QRM-20118 abdomen phantom, QRM) contained a cylindric core (QRM-10139 spectral CT phantom, QRM) designed for evaluation of spectral CT protocols; this core in turn contained refillable cylindric inserts, each having a diameter of 20 mm and length of 103 mm. The inserts were filled with increasing concentrations of gadoxetate disodium ranging from 0.00 to 2.5 μmol/mL in increments of 0.25 μmol/mL (i.e., double the increment used for the custom phantom).

The same originally prepared dilution series was used for both the custom and anthropomorphic phantoms. A second dilution series was independently created with the same target concentrations and evaluated using the custom phantom.

PCD CT Examinations

The CT examinations were performed using a clinically approved whole-body PCD CT system (NAEOTOM Alpha, VA50A, Siemens Healthineers). The custom phantom was intentionally scanned using parameters yielding high radiation doses to achieve high image quality, including low levels of image noise and artifacts: energy level of 120 kV, effective tube current–exposure time setting of 121, image quality level of 2600, pitch factor of 0.35, and rotation time of 0.5 seconds. Because the custom phantom included slots for 20 separate tubes, only a single acquisition was required to image all of the dilutions. In contrast, the anthropomorphic phantom was scanned separately for each dilution. The acquisitions for the anthropomorphic phantom used settings chosen to mimic a standard clinical abdominal protocol: energy level of 140 kV, effective tube current–exposure time setting of 35, image quality level of 90, pitch factor of 0.8, and rotation time of 0.5 seconds. All scans were performed in Quantum-plus mode, with acquisition of separate low- and high-energy information.

For the custom phantom, separate acquisitions were obtained for the two independently prepared dilution series. For the anthropomorphic phantom, each acquisition for the first dilution series was repeated three times. The $CTDI_{vol}$ was recorded for each acquisition.

Image Postprocessing and Analysis

From the acquisitions for both phantoms, spectral postprocessing datasets (i.e., datasets with intact low-energy-weighted and high-energy-weighted bins) were transferred to a workstation with dedicated local vendor postprocessing software (Syngo.via, version VB60, Siemens Healthineers). This workstation and software were used for all image analyses. Axial image sets were reconstructed using a Qr40 kernel with quantum iterative reconstruction (QIR) strength of 4, slice thickness of 5 mm, and an increment of 2 mm. Using a material decomposition algorithm, five image sets with these parameters were reconstructed for each concentration: 70-keV VMI, representing the mean energy level of a conventional energy-integrating detector (EID) CT scan at 120 kVp [23]; 40-keV, 50-keV, and 60-keV VMI, representing energy levels close to the K-edge for gadolinium and iodine, for relatively greater image contrast with respect to the 70-keV VMI; and virtual noncontrast (VNC) imaging, representing a negative control (i.e., absence of gadoxetate disodium). For the VNC imaging reconstruction, the material decomposition algorithm used an iodine ratio (i.e., the slope of the data points between the values for the high-energy-weighted and low-energy-weighted bins) that was adjusted for gadolinium (i.e., slope of 1.67 for 120-kVp scans in the custom phantom and 1.80 for 140-kVp scans in the anthropomorphic phantom) to optimize the removal of gadolinium from the images. For the custom phantom, separate image sets were also reconstructed for the low-energy-weighted and high-energy-weighted bins for each concentration.

A single investigator (S.R., 5th-year radiology resident) placed ROIs to obtain mean and SD values of attenuation measurements across the gadoxetate disodium concentrations in both phantoms.

Downloaded from www.ajronline.org by 186.248.128.23 on 05/21/25 from IP address 186.248.128.23. Copyright ARRS. For personal use only; all rights reserved

The investigator placed a single ROI in the center of each tube for the custom phantom and the center of each insert for the anthropomorphic phantom for all reconstructions, to obtain attenuation measurements across the gadoxetate disodium concentrations. The ROIs were of a similar size (diameter of approximately 10 mm) and location across all measurements. The mean and SD were recorded for each ROI. The mean values were in turn averaged between the two dilution series in the custom phantom and between the three repeated scans in the anthropomorphic phantom; the SD values were averaged in a similar manner, as an indicator of measurement noise. These averaged values were used for further analyses (aside from the scatterplot comparing measurements for each dilution series in the custom phantom, as described later in the Methods section). Finally, the postprocessing software was used to generate attenuation curves across the energy range from 40 to 190 keV for five representative concentrations (0.00, 0.25, 1.00, 1.75, and 2.50 µmol/mL) for the first dilution series in the custom phantom based on an ROI placed by the investigator in the original spectral postprocessing dataset.

Estimation of In Vivo Hepatic Attenuation and Enhancement

A simulation was performed to estimate in vivo hepatic attenuation and enhancement across gadoxetate disodium concentrations, based on the measurements in the anthropomorphic phantom. First, the theoretic concentration of gadoxetate disodium in hepatic parenchyma for a dose of 200 µmol/kg was estimated by matching the calculated increase in attenuation for this dose for 70-keV VMI (corresponding to the mean electron density for EID CT at 120 kVp) with the previously reported in vivo enhancement of the liver parenchyma of 13 HU at a gadoxetate disodium dose of 200 µmol/kg [10]. Based on the derived hepatic concentration of gadoxetate disodium for a dose of 200 µmol/kg, hepatic concentrations were approximated for lower doses of 25, 50, 75, and 100 µmol/kg. For this purpose, the hepatic concentration was initially calculated assuming a linear correlation. Then, to account for higher hepatic uptake of gadoxetate disodium at doses less than or equal to 100 µmol/kg (estimated uptake of 35% vs 45% for doses ≤ 100 µmol/kg vs > 100 µmol/kg, respectively), the initially calculated hepatic concentration was corrected by a factor of 1.29, resulting in the formula:

$$\textit{hepatic concentration}\,(x) = 200\,\frac{\mu mol}{kg} \times \frac{x}{200\,\frac{\mu mol}{kg}} \times 1.29, \qquad (1)$$

with x representing doses of gadoxetate disodium less than or equal to 100 µmol/kg body weight. This adjustment was based on studies of pharmacokinetics of gadoxetate disodium and related molecules (e.g., dysprosium-EOB-DTPA) in humans [10, 22, 24]; such studies revealed greater fecal excretion of gadoxetate disodium at doses great-

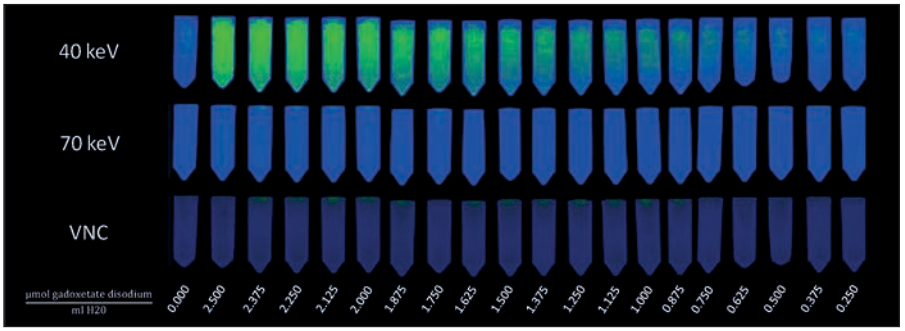

Fig. 2—Image from photon-counting detector CT shows gadoxetate disodium dilution series from custom phantom with 40-keV virtual monoenergetic imaging (VMI) (40 keV), 70-keV VMI (70 keV), and virtual noncontrast imaging (VNC) reconstructions.

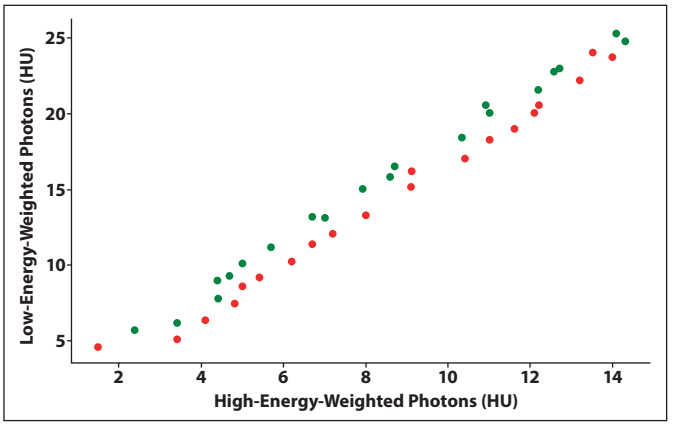

Fig. 3—Scatterplot shows attenuation measurements between low-energy-weighted and high-energy-weighted reconstructions from two independently prepared dilution series (A, *red dots,* and B, *green dots*) in custom phantom.

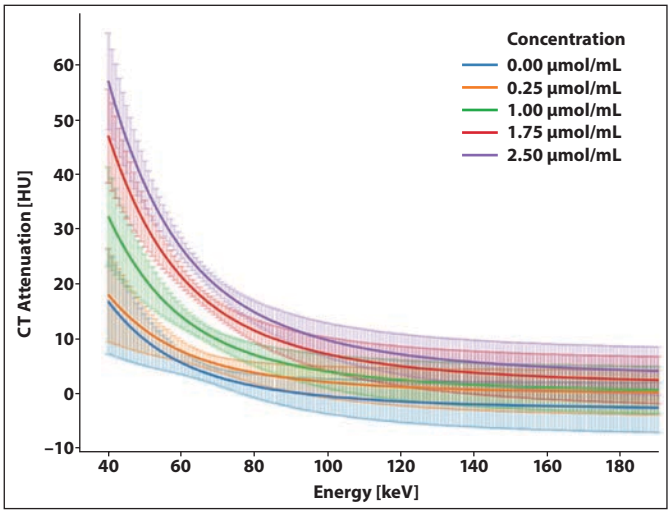

Fig. 4—Schematic shows attenuation curves across energy levels from 40 to 190 keV for five representative gadoxetate disodium concentrations in custom phantom. Vertical whiskers indicate the SD of the ROI measurement.

Downloaded from www.ajronline.org by 186.248.128.23 on 05/21/25 from IP address 186.248.128.23. Copyright ARRS. For personal use only; all rights reserved

Downloaded from www.ajronline.org by 186.248.128.23 on 05/21/25 from IP address 186.248.128.23. Copyright ARRS. For personal use only; all rights reserved

er than 100 μmol/kg, likely due to saturation of hepatocyte transporter molecules involved in the agent's intracellular uptake [9, 25].

Linear regression analyses were then performed to generate best-fit lines of attenuation as a function of gadoxetate disodium dose for 40-keV VMI and VNC imaging reconstructions in the anthropomorphic phantom. Subsequently, the hepatic enhancement, *HE*, for each derived hepatic concentration of gadoxetate disodium was calculated as the difference between the hepatic attenuation for the given concentration and the hepatic attenuation for deionized water; each such attenuation was in turn calculated as the difference in respective attenuation measurements between the 40-keV VMI and VNC imaging reconstructions, based on the best-fit regression lines. This process yielded an overall formula to determine *HE* for a given concentration *y* of:

$$HE\,(y) = \big(40\ keV(y) - VNC\,(y)\big) - (40\ keV\,(water) - VNC\,(water)\big), \quad (2)$$

To account for image noise in the anthropomorphic phantom, the CNR with respect to deionized water was calculated for each concentration *x* (Gd_x) based on attenuation measurements using the equation:

$$CNR_x = \frac{Gd_x - H_20}{\delta}, \quad (3)$$

with σ representing the previously noted summary SD value obtained from the ROI measurements.

Statistical Analysis

Percent deviation between expected gadolinium concentrations in the dilution series and measured gadolinium concentrations by mass spectroscopy were computed. Scatterplots were constructed comparing attenuation measurements from the low-energy-weighted and high-energy-weighted bins for each concentration from each of the two dilution series in the custom phantom. The mean and SD values for attenuation measurements for each combination of concentration and reconstruction in each phantom were tabulated. The mean and SD values of the attenuation measurements were plotted for the 40-keV VMI, 70-keV VMI, and VNC imaging reconstructions for the custom phantom, as well as for the 40-keV VMI and VNC imaging reconstructions for the anthropomorphic phantom. These plots were qualitatively characterized. The mean SDs of attenuation measurements across concentrations were compared between the custom and anthropomorphic phantoms using a paired *t* test. Linear regression analysis was used to interpolate missing values between measured data points, presuming linear relationships between adjacent measurements. The difference in estimated hepatic attenuation between the 40-keV VMI and VNC imaging reconstructions at each theoretic hepatic concentration was plotted in the anthropomorphic phantom. The results of the previously described analyses to estimate in vivo hepatic attenuation, enhancement, and CNR were further tabulated. The *p* value was considered statistically significant if less than 05. All statistical analyses were performed using Python (version 3.10.12).

Results

Initial Phantom Measurements

The phantom setups, image acquisitions, and image reconstructions were successfully completed. The mass spectroscopy measurements confirmed the validity of the dilution series, showing deviations between the expected and actual gadoxetate disodium concentrations ranging from −0.2% to 4.4% (Table 1). The mean $CTDI_{vol}$ for the custom phantom (scanned with high doses to reduce image noise) was 9.59 mGy. The mean $CTDI_{vol}$ of the anthropomorphic phantom (scanned with a clinical protocol) was 4.00 mGy.

TABLE 1: Mass Spectroscopy Measurements of Gadoxetate Disodium Concentrations in the Dilution Series in Comparison With the Expected Gadoxetate Disodium Concentration

Expected Value	Measured Value	Deviation From Expected Value (%)
0.000	0.000	—
0.250	0.261	4.4
0.375	0.374	−0.2
0.500	0.495	−1.1
0.625	0.634	1.4
0.750	0.777	3.7
0.875	0.899	2.7
1.000	1.027	2.7
1.125	1.155	2.6
1.250	1.277	2.2
1.375	1.420	3.2
1.500	1.562	4.1
1.625	1.653	1.7
1.750	1.802	3.0
1.875	1.919	2.4
2.000	2.052	2.6
2.125	2.135	0.5
2.250	2.303	2.3
2.375	2.387	0.5
2.500	2.498	−0.1

Figure 2 shows CT images of the custom phantom, with tubes containing the dilution series of gadoxetate disodium concentrations ranging from 0.00 to 2.500 μmol/mL for 40-keV VMI, 70-keV VMI, and VNC imaging reconstructions. Visual assessment of the images indicates greater attenuation for 70-keV VMI with respect to VNC imaging reconstructions and for 40-keV VMI with respect to 70-keV VMI reconstructions. Visual assessment also indicates increasing attenuation with increasing concentration for the 40-keV VMI reconstructions.

Figure 3 depicts the attenuation measurements for the low-energy-weighted and high-energy-weighted values for the two independently prepared dilution series in the custom phantom. The observed pattern is similar for the two series.

Attenuation Measurements Across Concentrations and Energy Levels

Figure 4 depicts attenuation curves from 40 to 190 keV for five representative gadoxetate disodium concentrations (0.00, 0.25,

TABLE 2: Attenuation Measurements for the Dilution Series in Virtual Monoenergetic and VNC Reconstructions in the Custom Phantom

Gadoxetate Disodium Concentration (μmol/mL)	40 keV	50 keV	60 keV	70 keV	VNC
0.000	13.5 ± 3.8	9.8 ± 3.5	6.0 ± 1.5	3.4 ± 1.4	–2.7 ± 1.5
0.250	11.1 ± 4.4	10.8 ± 3.6	7.4 ± 1.6	4.3 ± 1.0	0.3 ± 1.3
0.375	14.5 ± 3.8	11.9 ± 3.8	8.4 ± 1.8	5.7 ± 1.3	0.9 ± 1.4
0.500	17.6 ± 3.8	12.5 ± 3.7	8.5 ± 1.7	6.1 ± 1.3	1.0 ± 1.2
0.625	19.3 ± 3.9	14.3 ± 3.7	10.1 ± 1.7	6.9 ± 1.3	0.6 ± 1.3
0.750	21.0 ± 3.9	15.1 ± 3.3	10.2 ± 1.5	7.5 ± 1.2	0.5 ± 1.2
0.875	23.1 ± 3.8	16.3 ± 3.9	11.6 ± 1.8	8.4 ± 1.3	1.2 ± 1.3
1.000	26.5 ± 3.9	18.2 ± 3.8	12.8 ± 1.8	9.3 ± 1.3	1.1 ± 1.2
1.125	27.1 ± 3.9	19.2 ± 3.8	13.6 ± 1.8	9.7 ± 1.3	1.5 ± 1.3
1.250	30.2 ± 3.5	20.1 ± 3.8	14.3 ± 1.7	10.8 ± 1.2	2.1 ± 1.3
1.375	32.8 ± 3.5	23.0 ± 3.7	16.3 ± 1.7	11.7 ± 1.3	2.2 ± 1.3
1.500	35.2 ± 3.7	23.8 ± 3.9	17.0 ± 1.8	12.7 ± 1.2	2.4 ± 1.4
1.625	36.7 ± 3.9	25.9 ± 3.7	18.5 ± 1.7	13.7 ± 1.3	2.8 ± 1.2
1.750	40.9 ± 3.9	28.0 ± 3.8	19.9 ± 1.7	14.7 ± 1.3	2.9 ± 1.4
1.875	40.5 ± 4.1	27.9 ± 4.0	20.0 ± 1.8	15.0 ± 1.4	3.2 ± 1.5
2.000	43.6 ± 4.0	30.1 ± 3.8	21.7 ± 1.8	16.1 ± 1.3	3.6 ± 1.3
2.125	44.5 ± 3.9	32.8 ± 3.8	23.6 ± 1.8	16.5 ± 1.4	3.5 ± 1.3
2.250	47.0 ± 3.8	32.8 ± 3.8	23.6 ± 1.7	17.5 ± 1.3	4.0 ± 1.3
2.375	49.7 ± 4.2	35.1 ± 3.8	25.0 ± 1.7	18.4 ± 1.3	4.4 ± 1.4
2.500	52.6 ± 4.0	35.4 ± 3.6	25.1 ± 1.7	18.4 ± 1.3	2.9 ± 1.6

Note—Data represent Hounsfield units and are reported as mean ± SD. VNC = virtual noncontrast.

1.00, 1.75, and 2.50 μmol/mL) in the custom phantom. These curves indicate progressive increases in attenuation with increasing gadoxetate disodium concentration at a given energy level, as well as an exponential increase in attenuation as the energy level decreases toward 40 keV for a given concentration.

Figure 5 depicts the mean and SD values for the attenuation measurements across gadoxetate disodium concentrations for the 40-keV VMI, 70-keV VMI, and VNC imaging reconstructions in the custom phantom. For both 40-keV and 70-keV VMI reconstructions, a progressive increase in attenuation was observed with increasing concentrations, with a steeper slope of increase for the 40-keV VMI than for the 70-keV VMI reconstruction; the VNC imaging reconstruction showed no increase in attenuation with increasing concentration. At each concentration, attenuation was greater for 40-keV VMI than for 70-keV VMI and for 70-keV VMI than for the VNC imaging reconstruction. Table 2 summarizes attenuation measurements at each concentration for each reconstructed image set in the custom phantom, indicating increasing attenuation with increasing concentration or lower energy level. The maximum mean attenuation reached was 52.6 HU for a gadoxetate disodium concentration of 2.5 μmol/mL with 40-keV VMI. The solution with a concentration of 0.25 μmol/mL had a mean attenuation on 40-keV VMI of 11.1 HU. The solution with a concentration of 0.0 μmol/mL (i.e., deionized water) had a mean attenuation on VNC imaging of –2.7 HU.

Figure 6 depicts the mean and SD values for the attenuation measurements across gadoxetate disodium concentrations for the 40-keV VMI and VNC imaging reconstructions in the anthropomorphic phantom. As in the custom phantom, progressive increases in attenuation were observed with increasing concentration for the 40-keV VMI reconstruction but not for the VNC imaging reconstruction; at each concentration, attenuation was greater for 40-keV VMI than for the VNC imaging reconstructions. Table 3 summarizes attenuation measurements at each concentration for each reconstructed image set in the anthropomorphic phantom, indicating increasing attenuation with increasing concentration or lower energy level. The maximum mean attenuation reached was 45.2 HU for a gadoxetate disodium concentration of 2.5 μmol/mL at 40 keV. The solution with a concentration of 0.25 μmol/mL had a mean attenuation on 40-keV VMI of 13.0 HU. The solution with a concentration of 0.0 μmol/mL had a mean attenuation on VNC imaging of –15.6 HU.

Image noise was substantially greater for the anthropomorphic phantom than for the custom phantom, as indicated by greater SDs, particularly for the 40-keV VMI reconstruction (mean SD across all concentrations at 40 keV of 38.2 vs 3.9 HU; $p < .001$). For concentrations evaluated by both the custom and anthropomorphic phantoms, although all mean attenuation values differed between the two phantoms, the mean attenuation values in the custom phantom were all within 1 SD of the mean attenuation values in the anthropomorphic phantom at this energy level.

Downloaded from www.ajronline.org by 186.248.128.23 on 05/21/25 from IP address 186.248.128.23. Copyright ARRS. For personal use only; all rights reserved

Downloaded from www.ajronline.org by 186.248.128.23 on 05/21/25 from IP address 186.248.128.23. Copyright ARRS. For personal use only; all rights reserved

Simulation to Estimate In Vivo Hepatic Attenuation and Enhancement With Gadoxetate Disodium

Based on a combination of attenuation measurements in the anthropomorphic phantom and prior literature-reported data, a gadoxetate disodium dose of 200 μmol/kg was estimated to correspond to a theoretic hepatic gadoxetate disodium concentration of 2.25 μmol/mL, and lower doses of 25–100 μmol/kg were estimated to correspond with theoretic hepatic concentrations of 0.36–1.45 μmol/mL. Figure 7 depicts estimated hepatic attenuation (i.e., difference in attenuation between 40-keV virtual monoenergetic and VNC images) at each derived gadoxetate disodium hepatic concentration.

Table 4 summarizes the estimated in vivo hepatic enhancement (i.e., difference in hepatic attenuation between the given gadoxetate disodium dose and deionized water) for gadoxetate disodium doses at 40 keV, determined using results from linear regression analyses. Based on this model, the estimated in vivo hepatic enhancement at 40 keV was 4.9 HU for a dose of 25 μmol/kg (i.e., the standard clinical dose), 19.9 HU for 100 μmol/kg, and 30.8 HU for 200 μmol/kg. Table 4 also provides CNR values for each gadoxetate disodium dose. For doses of 25, 100, and 200 μmol/kg, the CNR was 0.13, 0.52, and 0.81, respectively.

Discussion

In this phantom study, we systematically investigated dose-dependent increases in attenuation for gadoxetate disodium imaged by a whole-body PCD CT system with low-energy VMI reconstructions. Gadoxetate disodium in clinically approved doses did not yield meaningful attenuation increases. However, based on simulations using the phantom measurements to estimate hepatic attenuation in humans, the combination of gadoxetate disodium and PCD CT would theoretically allow appreciable hepatic enhancement, as indicated by a CNR of 0.81 at a dose of 200 μmol/kg. Nonetheless, such a dose is approximately eightfold higher than the current clinically approved dose of gadoxetate disodium of 25 μmol/kg.

GBCAs have low permitted doses in current clinical practice, given possible acute and chronic side effects as well as concern for nephrogenic systemic fibrosis (NSF) and gadolinium retention in various tissues [23, 26–28]. However, limited data support the potential feasibility of the larger doses. In clinical trials, twofold and fourfold doses of gadoxetate disodium (50 μmol/kg and 100 μmol/kg, respectively) were not associated with increases in adverse reactions in small numbers of patients [24–26, 29]. An additional study described side effects after injection of even higher

TABLE 3: Attenuation Measurements for the Dilution Series in Virtual Monoenergetic and VNC Reconstructions in the Anthropomorphic Abdominal Phantom

Gadoxetate Disodium Concentration (μmol/mL)	40 keV	50 keV	60 keV	70 keV	VNC
0.00	14.7 ± 40.4	6.6 ± 26.2	2.3 ± 18.5	−0.2 ± 12.6	−15.6 ± 10.0
0.25	13.0 ± 37.5	6.9 ± 24.8	3.5 ± 17.1	1.4 ± 12.2	−11.3 ± 9.3
0.50	13.9 ± 37.5	6.8 ± 26.0	3.8 ± 17.3	2.2 ± 10.7	−10.3 ± 9.13
0.75	19.0 ± 38.7	11.0 ± 25.5	6.5 ± 17.5	3.8 ± 11.9	−10.2 ± 9.9
1.00	20.0 ± 40.0	13.4 ± 24.7	8.4 ± 17.0	4.8 ± 11.1	−7.4 ± 9.5
1.25	26.5 ± 35.9	16.6 ± 23.8	10.4 ± 16.6	6.5 ± 12.1	−8.6 ± 9.8
1.50	30.4 ± 37.7	18.9 ± 24.6	12.1 ± 17.0	8.4 ± 11.9	−10.3 ± 9.7
1.75	36.9 ± 38.3	23.1 ± 25.4	14.8 ± 17.3	10.4 ± 12.1	−13.0 ± 9.7
2.00	38.7 ± 37.7	25.0 ± 25.0	16.7 ± 17.1	11.2 ± 11.5	−9.8 ± 9.7
2.25	42.7 ± 37.7	26.7 ± 25.4	18.0 ± 17.4	12.7 ± 11.8	−11.5 ± 9.6
2.50	45.2 ± 38.3	28.4 ± 25.2	19.9 ± 17.2	13.6 ± 12.2	−11.0 ± 10.3

Note—Data represent Hounsfield units and are reported as mean ± SD. VNC = virtual noncontrast.

TABLE 4: Estimated In Vivo Hepatic Enhancement and CNR for Different Doses and Corresponding Theoretic Hepatic Concentrations of Gadoxetate Disodium, Based on Results in the Anthropomorphic Phantom

Gadoxetate Disodium Dose (μmol/kg body weight)	Theoretic Hepatic Concentration of Gadoxetate Disodium (μmol/mL)	Estimated In Vivo Hepatic Enhancement (HU)[a]	CNR
25	0.36	4.9 ± 38.0	0.13
50	0.73	10.0 ± 39.0	0.26
75	1.09	14.9 ± 40.0	0.37
100	1.45	19.9 ± 38.0	0.52
200	2.25	30.8 ± 38.0	0.81

Note—Hepatic enhancement was estimated by comparing liver attenuation with that of deionized water.
[a]Reported as mean ± SD.

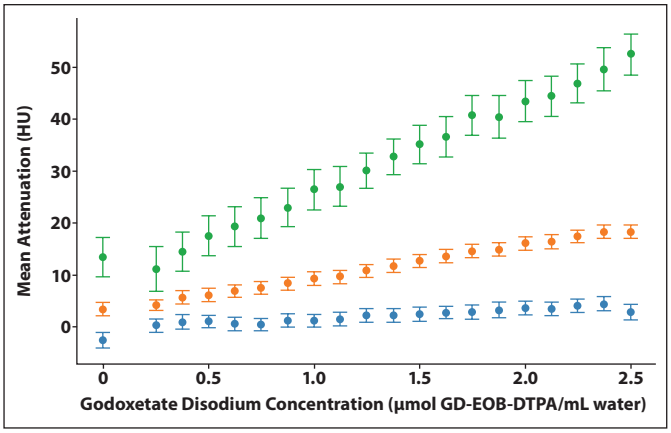

Fig. 5—Schematic shows mean attenuation values for different gadoxetate disodium concentrations in custom phantom for 40-keV virtual monoenergetic imaging (VMI) reconstruction (*green*), 70-keV VMI reconstruction (*red*), and virtual noncontrast (VNC) imaging reconstruction (*blue*). Dots indicate mean of two independently prepared dilution series; vertical lines indicate error bars.

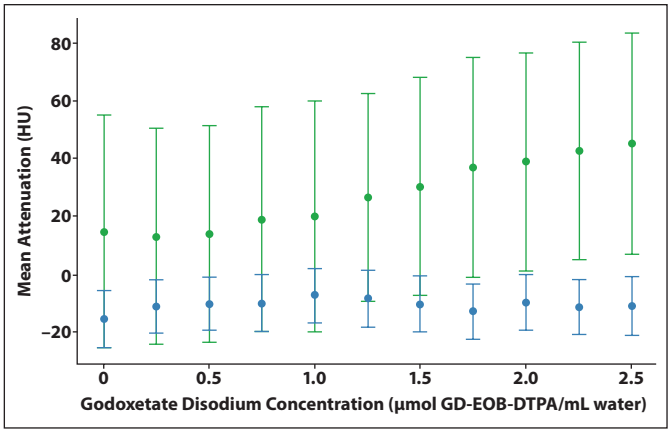

Fig. 6—Schematic shows mean attenuation values for different gadoxetate disodium concentrations in anthropomorphic phantom for 40-keV virtual monoenergetic imaging (*green*) and virtual noncontrast imaging (*blue*) reconstructions. Dots indicate mean of three repeated acquisitions; vertical lines indicate error bars.

doses of gadoxetate disodium of 200–500 μmol/kg including mild nausea, right upper quadrant discomfort, and burning sensations, yet considered these doses to be associated with acceptable tolerance [10]. Furthermore, no cases of NSF related to gadoxetate disodium have been reported [30–33]. Nonetheless, systematic safety investigations on high doses of gadoxetate disodium remain lacking, and the high doses found in this study to potentially achieve hepatic enhancement in combination with PCD CT cannot be adopted in the absence of further safety evidence.

Future investigations should seek to optimally leverage the benefits of PCD technology for gadolinium-enhanced imaging. For example, artificial intelligence could be used to refine postprocessing algorithms to achieve improved visualization of gadolinium (e.g., through improved denoising and subsequent higher CNR). If additional research and development could reduce further the doses of gadoxetate disodium required to achieve meaningful hepatic enhancement with PCD CT into a clinically acceptable level (even if still higher than current clinical doses), then this combination could hold potential in various clinical settings. For example, the approach could be useful for liver evaluation in settings in which MRI is unavailable, in patients unable to undergo MRI, and in patients with a history of severe allergic reactions to iodine-based contrast agents. The availability of a hepatocyte-specific CT contrast agent would also be beneficial given the rapid washout of iodine-based agents; the prolonged enhancement resulting from such agents aids visualization of certain liver-specific structures and pathologies, with potentially improved detection and characterization of a spectrum of benign and malignant liver conditions. Additionally, for patients undergoing CT-guided liver biopsy or other liver interventions, a hepatocyte-specific contrast agent could improve procedural accuracy by providing long-lasting delineation of target lesions. Furthermore, the ability to perform quantitative analysis of liver function or regional liver perfusion with a hepatocyte-specific agent would provide complementary anatomic and functional information, as is more commonly obtained by MRI. These potential applications of gadoxetate disodium, regardless of dose, would be challenged in patients with liver failure, as adequate liver function is critical for the agent's hepatic excretion and consequent hepatic enhancement [34].

A number of limitations impact the present findings' potential clinical translation. First, the attenuation curves in the custom phantom progressively increased as the energy level decreased toward 40 keV and thus diverged from anticipated physical absorp-

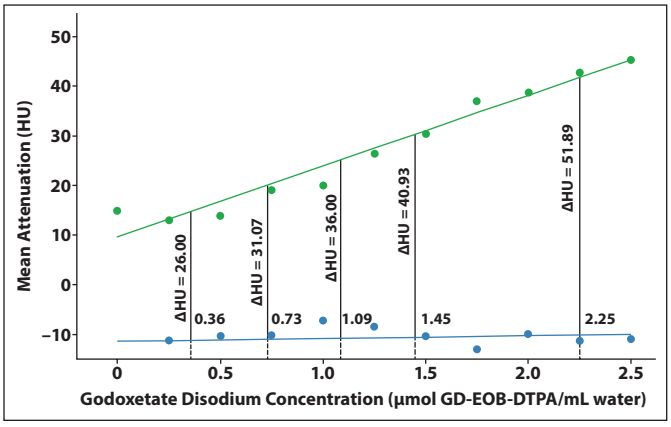

Fig. 7—Graph shows estimated in vivo hepatic measurements using data from anthropomorphic phantom. Green (40-keV virtual monoenergetic imaging) and blue (virtual noncontrast [VNC] imaging) lines represent best-fit lines from linear regression analyses of mean attenuation values (*dots*) to gadoxetate disodium concentrations. Vertical black lines indicate estimated hepatic attenuation values (expressed as difference in attenuation between 40 keV and VNC reconstructions) at theoretic hepatic gadoxetate disodium concentrations. These hepatic attenuation values of gadoxetate disodium were in turn used in combination with hepatic attenuation values for deionized water to estimate hepatic enhancement (see Table 4).

Downloaded from www.ajronline.org by 186.248.128.23 on 05/21/25 from IP address 186.248.128.23. Copyright ARRS. For personal use only; all rights reserved

Downloaded from www.ajronline.org by 186.248.128.23 on 05/21/25 from IP address 186.248.128.23. Copyright ARRS. For personal use only; all rights reserved

tion curves for gadolinium, which would be expected to show a peak at gadolinium's K-edge of 50.2 keV [11]. This deviation can be attributed to the spectral postprocessing software, which is tailored to iodine, characterized by a lower electron density and lower K-edge of 33.2 keV [2]. Consistent with other dual-energy CT scanners, the PCD CT system generates VMI reconstructions based on material decomposition into water and iodine, such that gadolinium is expressed as an iodine-water mixture. However, for uncertain reasons, gadoxetate disodium exhibited higher attenuation at a low-energy level for PCD CT compared with findings from prior phantom studies using earlier-generation dual-energy CT systems. For example, attenuation in the anthropomorphic phantom for a concentration of 2.5 μmol/mL at 40 keV was approximately 45 HU, versus comparable values of 20–28 HU from earlier literature [35–38]. PCD CT postprocessing algorithms could be adapted to account for the specific attenuation characteristics of GBCAs and thereby improve the precision of attenuation measurements, particularly at low energy levels, for such agents.

Characteristics of the spectral acquisition may also have impacted precision of the attenuation measurements, causing potential deviations from attenuation measurements that may be encountered in clinical settings. In particular, the PCD CT scanner used in this study had only two available energy bins for direct measurement, such that spectral postprocessing with material decomposition was required to generate VMI reconstructions at various energy levels. PCD technology has the potential to acquire multispectral data using up to four energy bins, although such acquisitions are currently possible only using dedicated research software. Implementation of additional energy thresholds and appropriate energy threshold weighting could facilitate better discrimination, especially of low-energy photons, to yield improved image contrast [39]. An extension of multispectral acquisition that could potentially further improve image contrast is so-called K-edge imaging, whereby one energy threshold is positioned close to the material's K-edge.

Another limitation relates to the challenge of visualizing water by PCD CT, particularly in terms of calibration offsets. The dilution with a concentration of 0.00 μmol/mL (i.e., deionized water) exhibited an attenuation for the VNC imaging reconstruction in the custom phantom of –2.7 HU, not the expected value of 0.0 HU. This error's exact cause is uncertain, although it likely represents systematic postprocessing issues. This discrepancy was observed despite the software's use of a gadolinium-specific slope for the VNC imaging reconstructions. The VNC imaging reconstructions were consistently used to provide baseline attenuation values when estimating in vivo hepatic enhancement at 40 keV, partly addressing this issue.

Several additional limitations warrant mention. First, hepatocyte-specific GBCAs have more heterogeneous distribution throughout the body than in phantom tubes or inserts, being influenced by liver perfusion and function with particular regard to potential transporter saturations in hepatocytes and other possible influences like blood flow and renal function [9, 24]. Also, mean attenuation values for the 40-keV VMI reconstructions differed between the two phantoms, likely relating to the substantially higher image noise in the anthropomorphic phantom. Nonetheless, the mean values from the custom phantom were all within 1 SD of the mean values from the anthropomorphic phantom. Finally, the nonlinear nature of the applied iterative reconstruction algorithm limits the validity of CNR as a comparative measure of conspicuity among different image sets [40].

In conclusion, the use of PCD CT with low-energy VMI reconstructions achieved attenuation increases for gadoxetate disodium at considerably lower doses than previously documented for CT of GBCA, albeit at approximately eight times greater than clinical doses and thus too high for clinical use. Similar attenuation increases were not observed for standard clinical doses. Additional research exploiting currently available PCD CT systems should seek to reduce further the dose of gadoxetate disodium required to achieve sufficient visualization into a clinically feasible range.

Provenance and review: Not solicited; externally peer reviewed.

Peer reviewers: Yoshito Tsushima, Gunma University; Xinyan Zhou, Yan'an Hospital of Kunming City; Amir A. Borhani, Northwestern University Feinberg School of Medicine; Nobuo Tomizawa, Yan'an Hospital of Kunming City; additional individual(s) who chose not to disclose their identity.

CME: ARRS is accredited by the Accreditation Council for Continuing Medical Education (ACCME) to provide continuing medical education activities for physicians. The ARRS designates this journal-based CME activity for a maximum of 1.00 AMA PRA Category 1 Credit™. Physicians should claim only the credit commensurate with the extent of their participation in the activity.

References

1. Caschera L, Lazzara A, Piergallini L, Ricci D, Tuscano B, Vanzulli A. Contrast agents in diagnostic imaging: present and future. *Pharmacol Res* 2016; 110:65–75
2. National Institute of Standards and Technology. X-ray mass attenuation coefficients: iodine. physics.nist.gov/PhysRefData/XrayMassCoef/ElemTab/z53.html. Accessed Apr 19, 2024
3. Beckett KR, Moriarity AK, Langer JM. Safe use of contrast media: what the radiologist needs to know. *RadioGraphics* 2015; 35:1738–1750
4. Bae KT. Intravenous contrast medium administration and scan timing at CT: considerations and approaches. *Radiology* 2010; 256:32–61
5. Remy-Jardin M, Dequiedt P, Ertzbischoff O, et al. Safety and effectiveness of gadolinium-enhanced multi-detector row spiral CT angiography of the chest: preliminary results in 37 patients with contraindications to iodinated contrast agents. *Radiology* 2005; 235:819–826
6. Esteban JM, Alonso A, Cervera V, Martínez V. One-molar gadolinium chelate (gadobutrol) as a contrast agent for CT angiography of the thoracic and abdominal aorta. *Eur Radiol* 2007; 17:2394–2400
7. Cheong BYC, Wilson JM, Preventza OA, Muthupillai R. Gadolinium-based contrast agents: updates and answers to typical questions regarding gadolinium use. *Tex Heart Inst J* 2022; 49:e217680
8. Boccalini S, Dessouky R, Rodesch PA, et al. Gadolinium K-edge angiography with a spectral photon counting CT in atherosclerotic rabbits. *Diagn Interv Imaging* 2023; 104:490–499
9. Krause W, Mahler M, Hanke B, et al. Dy-EOB-DTPA: tolerance and pharmacokinetics in healthy volunteers and preliminary liver imaging in patients. *Invest Radiol* 2001; 36:431–444
10. Schmitz SA, Häberle JH, Balzer T, Shamsi K, Boese-Landgraf J, Wolf KJ. Detection of focal liver lesions: CT of the hepatobiliary system with gadoxetic acid disodium, or Gd-EOB-DTPA. *Radiology* 1997; 202:399–405
11. National Institute of Standards and Technology. X-ray mass attenuation coefficients: gadolinium oxysulfide. physics.nist.gov/PhysRefData/XrayMassCoef/ComTab/gadolinium.html. Accessed Apr 19, 2024
12. Thomsen HS. Guidelines for contrast media from the European Society of Urogenital Radiology. *AJR* 2003; 181:1463–1471
13. Yanaga Y, Awai K, Nakaura T, et al. Optimal contrast dose for depiction of hypervascular hepatocellular carcinoma at dynamic CT using 64-MDCT.

AJR 2008; 190:1003–1009
14. Caruso D, De Santis D, Del Gaudio A, et al. Lean body weight-based contrast injection protocol in liver CT: optimization of contrast medium dose. *Radiol Med (Torino)* 2024 Dec 30 [published online]
15. Zanardo M, Doniselli FM, Esseridou A, et al. Abdominal CT: a radiologist-driven adjustment of the dose of iodinated contrast agent approaches a calculation per lean body weight. *Eur Radiol Exp* 2018; 2:41
16. Bayer. Primovist. (product monograph) www.bayer.com/sites/default/files/2020-11/primovist-pm-en.pdf. Revised Jun 14, 2024. Accessed Apr 19, 2024
17. Jost G, McDermott M, Gutjahr R, Nowak T, Schmidt B, Pietsch H. New contrast media for K-edge imaging with photon-counting detector CT. *Invest Radiol* 2023; 58:515–522
18. Schwartz FR, Samei E, Marin D. Exploiting the potential of photon-counting CT in abdominal imaging. *Invest Radiol* 2023; 58:488–498
19. Bae KT. Intravenous contrast medium administration and scan timing at CT: considerations and approaches. *Radiology* 2010; 256:32–61
20. Frydrychowicz A, Lubner MG, Brown JJ, et al. Hepatobiliary MR imaging with gadolinium-based contrast agents. *J Magn Reson Imaging* 2012; 35:492–511
21. Schieda N, van der Pol CB, Walker D, et al. Adverse events to the gadolinium-based contrast agent gadoxetic acid: systematic review and meta-analysis. *Radiology* 2020; 297:565–572
22. Dahlström N. Quantitative evaluation of contrast agent dynamics in liver MRI. (dissertation) Linköping University, 2010
23. Shapira N, Mei K, Noël PB. Spectral CT quantification stability and accuracy for pediatric patients: a phantom study. *J Appl Clin Med Phys* 2021; 22:16–26
24. Motosugi U, Ichikawa T, Sano K, et al. Double-dose gadoxetic acid-enhanced magnetic resonance imaging in patients with chronic liver disease. *Invest Radiol* 2011; 46:141–145
25. Reimer P, Rummeny EJ, Shamsi K, et al. Phase II clinical evaluation of Gd-EOB-DTPA: dose, safety aspects, and pulse sequence. *Radiology* 1996; 199:177–183
26. Choi YM, John CS. NDA 22-090: clinical pharmacology review(s). Center for Drug Evaluation and Research. www.accessdata.fda.gov/drugsatfda_docs/nda/2008/022090s000_ClinPharmR.pdf. Submitted 2008. Accessed Apr 19, 2024
27. Kahn J, Posch H, Steffen IG, et al. Is there long-term signal intensity increase in the central nervous system on T1-weighted images after MR imaging with the hepatospecific contrast agent gadoxetic acid? A cross-sectional study in 91 patients. *Radiology* 2017; 282:708–716
28. Turyanskaya A, Rauwolf M, Pichler V, et al. Detection and imaging of gadolinium accumulation in human bone tissue by micro- and submicro-XRF. *Sci Rep* 2020; 10:6301
29. Hamm B, Staks T, Mühler A, et al. Phase I clinical evaluation of Gd-EOB-DTPA as a hepatobiliary MR contrast agent: safety, pharmacokinetics, and MR imaging. *Radiology* 1995; 195:785–792
30. Schuhmann-Giampieri G. Liver contrast media for magnetic resonance imaging. Interrelations between pharmacokinetics and imaging. *Invest Radiol* 1993; 28:753–761
31. Högemann D, Baumann A, Rocker D, Bader A, Galanski M. In vitro model of the human liver parenchyma to study hepatotoxic side effects by Dy-EOB-DTPA. *Invest Radiol* 2000; 35:373–379
32. Starekova J, Bruce RJ, Sadowski EA, Reeder SB. No cases of nephrogenic systemic fibrosis after administration of gadoxetic acid. *Radiology* 2020; 297:556–562
33. Lauenstein T, Ramirez-Garrido F, Kim YH, et al. Nephrogenic systemic fibrosis risk after liver magnetic resonance imaging with gadoxetate disodium in patients with moderate to severe renal impairment: results of a prospective, open-label, multicenter study. *Invest Radiol* 2015; 50:416–422
34. Tamada T, Ito K, Higaki A, et al. Gd-EOB-DTPA-enhanced MR imaging: evaluation of hepatic enhancement effects in normal and cirrhotic livers. *Eur J Radiol* 2011; 80:e311–e316
35. van Hamersvelt RW, Willemink MJ, de Jong PA, et al. Feasibility and accuracy of dual-layer spectral detector computed tomography for quantification of gadolinium: a phantom study. *Eur Radiol* 2017; 27:3677–3686
36. Bongers MN, Schabel C, Krauss B, Claussen CD, Nikolaou K, Thomas C. Potential of gadolinium as contrast material in second generation dual energy computed tomography: an ex vivo phantom study. *Clin Imaging* 2017; 43:74–79
37. Gabbai M, Leichter I, Mahgerefteh S, Sosna J. Spectral material characterization with dual-energy CT: comparison of commercial and investigative technologies in phantoms. *Acta Radiol* 2015; 56:960–969
38. Fält T, Söderberg M, Wassélius J, Leander P. Material decomposition in dual-energy computed tomography separates high-Z elements from iodine, identifying potential contrast media tailored for dual contrast medium examinations. *J Comput Assist Tomogr* 2015; 39:975–980
39. Willemink MJ, Persson M, Pourmorteza A, Pelc NJ, Fleischmann D. Photon-counting CT: technical principles and clinical prospects. *Radiology* 2018; 289:293–312
40. Vaishnav JY, Jung WC, Popescu LM, Zeng R, Myers KJ. Objective assessment of image quality and dose reduction in CT iterative reconstruction. *Med Phys* 2014; 41:071904

Downloaded from www.ajronline.org by 186.248.128.23 on 05/21/25 from IP address 186.248.128.23. Copyright ARRS. For personal use only; all rights reserved